

On the use of lithogenic tracer measurements in aerosols to constrain dust deposition fluxes to the ocean southeast of Australia.

Claudia Hird ^{a*}, Morgane M.G. Perron ^{ab*}, Thomas M. Holmes ^{c*}, Scott Meyerink ^c, Christopher Nielsen ^a, Ashley T. Townsend ^d, Patrice de Caritat ^e, Michal Strzelec ^a, Andrew R. Bowie ^{ac}

a Institute for Marine and Antarctic Studies (IMAS), University of Tasmania, Battery Point, Tasmania, Australia.

b Université de Brest - UMR 6539 CNRS/UBO/IRD/Ifremer, Laboratoire des sciences de l'environnement marin (LEMAR) - Institut Universitaire Européen de la Mer - Rue Dumont D'Urville, 29280 Plouzané, France

c Australian Antarctic Program Partnership (AAPP), University of Tasmania, Battery Point, Tasmania, Australia.

d Central Science Laboratory, University of Tasmania, Hobart, Tasmania, Australia

e John de Laeter Centre, Curtin University, Bentley WA 6845, Australia

* These authors contributed equally to this work.

Correspondence to: Morgane M.G. Perron, morgane.perron@univ-brest.fr

Abstract

1 Australia contributes a significant amount of dust-borne nutrients (including iron) to the Southern
2 Ocean, which can stimulate marine primary productivity. A quantitative assessment of the
3 variability of dust fluxes from Australia to the surrounding ocean is therefore important for
4 investigating the impact of atmospheric deposition on the Southern Ocean's carbon cycle. In this
5 study, lithogenic trace metals (aluminium, iron, thorium and titanium) contained in aerosols
6 collected between 2016 and 2021 from kunanyi/Mount Wellington in lutruwita/Tasmania
7 (Australia) were used to estimate dust deposition fluxes. Lithogenic fluxes were calculated using
8 each tracer individually, as well as an average using all four tracers. This latter approach enabled
9 an assessment of the uncertainty associated with flux calculations using only individual tracers.
10 Elemental ratios confirmed the lithogenic nature of each tracer in aerosols when compared with
11 both Australian soil samples and the average Earth's upper continental crust. Lithogenic flux
12 estimates showed annual dust deposition maxima during the austral summer, following the
13 Australian dust storm season, and annual minimum deposition flux over winter. The data provided

14 here will help to constrain model estimates of southern hemisphere atmospheric deposition fluxes
15 and their subsequent impact on global ocean biogeochemical cycles.

16

17 **Environmental significance / Plain language summary**

18 Dust deposition flux was investigated in lutruwita/Tasmania, Australia, between 2016 and 2021.
19 Results show that the use of direct measurement of aluminium, iron, thorium and titanium in
20 aerosols to estimate average dust deposition fluxes limits biases associated with using single
21 elements. Observations of dust deposition fluxes in the Southern Hemisphere are critical to
22 validate model outputs and better understand the seasonal and interannual impacts of dust
23 deposition on biogeochemical cycles.

24 **1. Introduction**

25 Lithogenic mineral particles such as iron oxyhydroxides, kaolinite, illite and smectite are
26 commonly entrained into the atmosphere (Cudahy et al., 2016) following the erosion of the Earth's
27 Upper Continental Crust (UCC) (Crawford et al., 2021). Such dust particles are the primary source
28 of trace metals including aluminium (Al), iron (Fe), thorium (Th) and titanium (Ti) to the
29 atmosphere, which can therefore be used as tracers of aeolian lithogenic inputs to the ocean (Baker
30 et al., 2020). Dust carries important nutrients, including Fe, to marine ecosystems, feeding primary
31 producers (Mackie et al., 2008). Due to the current lack of field observations on the concentrations
32 of aeolian trace metals and their corresponding dust deposition fluxes, large uncertainties remain
33 regarding how and to what extent dust supply fertilises key oceanic regions such as the Southern
34 Ocean with vital nutrients. This leads to a poor understanding of the impact of dust deposition on
35 the biological carbon pump.

36

37 The amount of dust entrained into the atmosphere depends on soil surface roughness, vegetation
38 and coverage, on particle size, composition, and moisture content, and on local conditions such as
39 wind speed and rainfall, which change both regionally and seasonally (Mahowald et al., 2009). Air
40 masses can carry dust over thousands of kilometres before particles return to land or fall onto the
41 surface ocean (Mackie et al., 2008). Atmospheric deposition of dust to the open ocean has been
42 demonstrated to act as a key supplier of vital macro- and micro-nutrients (such as Fe) to the marine
43 ecosystem (Mackie et al., 2008; Weis et al., 2024). For example, during the austral summer 2019-

44 2020, nutrient supply from large dust-containing bushfire emissions (Perron et al., 2022; Hamilton
45 et al., 2022) was identified as the main trigger of a large and long-lasting phytoplankton bloom in
46 the South Pacific Ocean (Weis et al., 2022).

47
48 Field and modelling approaches to estimating dust deposition both offer various benefits and
49 drawbacks. Field observations at sea are influenced by local environmental conditions (i.e.,
50 weather, surface ocean properties) and are not representative of the large scale or long-term
51 atmospheric deposition trends (Anderson et al., 2016). Time-series stations on land can overcome
52 the issue of temporal coverage but may not be representative of atmospheric loading and
53 deposition over remote oceanic regions. To date, global models are not capable of reproducing
54 atmospheric concentrations of trace metals transported in dust to remote areas and cannot
55 accurately quantify particle settling rates (Anderson et al., 2016). Considering the Southern
56 Hemisphere, model estimates tend to overestimate total dust emission at the source and
57 underestimate soluble trace element deposition fluxes over the ocean (Anderson et al., 2016; Ito et
58 al., 2020). To reduce uncertainty in dust deposition fluxes to the open ocean it is essential to
59 validate model fluxes using field-based observations. Long-term atmospheric observatories,
60 particularly near the coasts, are attracting increasing interest from the scientific community as a
61 platform to better understand seasonal to interannual patterns of deposition events in addition to
62 shipboard observations and satellite estimates (Perron et al., 2022; De Deckker, 2019).

63
64 In Australia, the large spatial heterogeneity of soil types and the highly episodic nature of weather
65 events such as droughts, bushfires and dust storms make it particularly difficult to model dust
66 deposition fluxes (Mackie et al., 2008), though modern dust emissions from South Australia have
67 been observed as far as the snow sheet of inner Antarctica (Vecchio et al., 2024). A main source
68 of trace metals to the Australian sector of the Southern Ocean is dust carried from kati thanda/Lake
69 Eyre and dhungala-barka/Murray-Darling geological basins (De Deckker, 2019). The typical dust
70 storm season in Australia spans from September to November (austral spring), with the most
71 extreme storms occurring in September (O’Loingsigh et al., 2017). The dust season can extend
72 through the austral summer due to bushfires (and postfire unvegetated ground) across southern
73 Australia (Hamilton et al., 2022). In a study conducted by Perron et al. (2022), atmospheric
74 concentrations of mineral dust and associated lithogenic tracers (Al, Fe and Ti) were reported to

75 be 2.5-fold higher, on average, during fire events compared to days not impacted by bushfires in
76 lutruwita/Tasmania, Australia.

77
78 Dust deposition fluxes reported by different models range over an order of magnitude (from 0.55
79 to 5.48 mg m⁻² d⁻¹) over the Southern Ocean region southeast of Australia (Mahowald et al., 2006;
80 Weis et al., 2024). Different methods have also been used to estimate dust deposition fluxes from
81 field samples. While broadly used in air pollution studies (Bindu et al., 2016), total aerosol loading
82 measurements based on gravimetry does not enable the discrimination of atmospheric sources
83 (e.g., dust vs anthropogenic). In addition, such a method is not compatible with atmospheric trace
84 metal studies, where strict protocol requires minimal filter handling to prevent contamination. from
85 the analysis of a single tracer element, for example Al or Th, in aerosol samples and in seawater
86 (Anderson et al., 2016). However, single element dust flux estimates are subject to anomalous data
87 stemming from contamination, deviation from the mean UCC, or preferential mineralization
88 following a particular laboratory protocol. Recently, the analysis of four lithogenic tracers
89 (namely, Al, Fe, Th, and Ti) in marine sinking particles collected at the Southern Ocean Time-
90 Series (SOTS) mooring station (140°E, 47°S) were used to calculate an average ‘multi-tracer’
91 estimate of dust deposition fluxes to surface waters of the subantarctic ocean south of Australia
92 (Traill et al., 2022). The latter field-based flux estimates showed good agreement with remotely
93 sensed proxies of dust transport and modelled deposition estimates. Elemental ratio analysis in the
94 same sediment trap samples suggested that lithogenic material from southeastern Australia was
95 the most likely source of Al, Fe, Th and Ti to this area of the Southern Ocean (Traill et al., 2022).

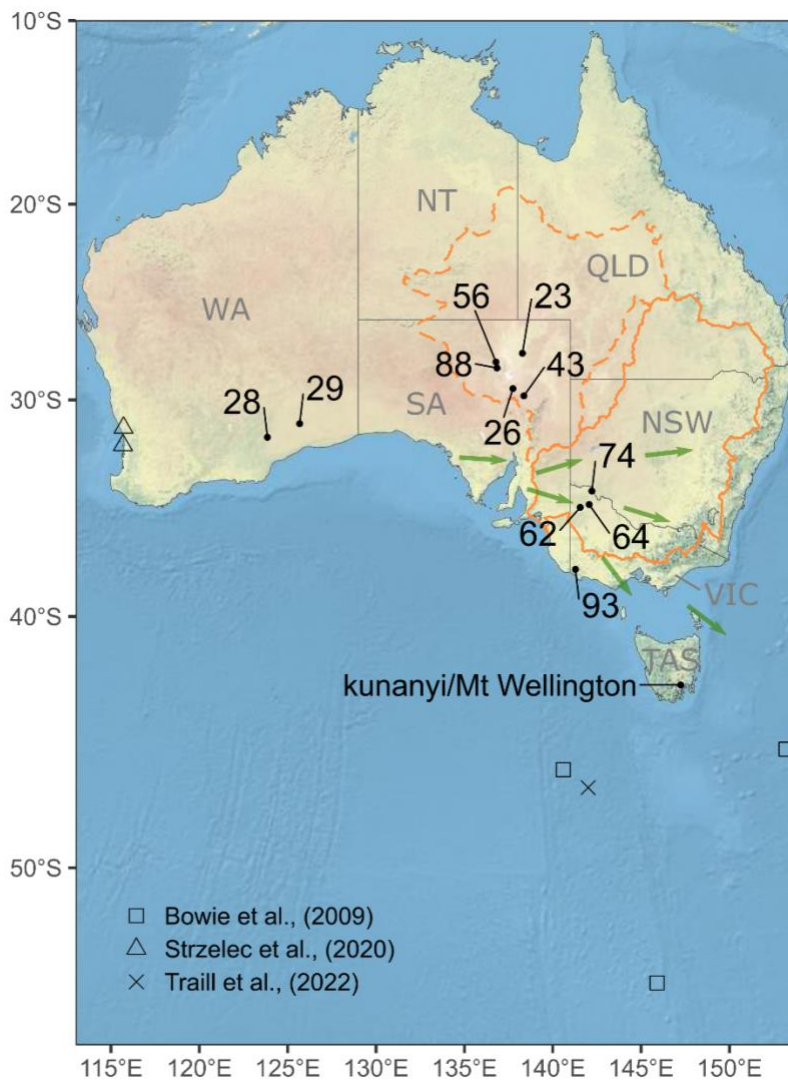
96
97 In this study, the analysis of the same four lithogenic tracers (Al, Fe, Th, and Ti) was performed
98 in aerosol samples collected at the kunanyi/Mount Wellington time-series sampling station in
99 southern lutruwita/Tasmania (Australia). Dust deposition fluxes were estimated from both
100 individual tracer concentrations and using the multi-tracer approach used by Traill et al. (2022).
101 Here we report a 5-year (2016-2021) time-series of dust deposition flux estimates downwind of
102 the south-eastern Australian dust path, at one of the gateway to the Southern Ocean. The suitability
103 of the four metals as lithogenic tracers was also verified by comparing elemental ratios (relative to
104 Al) in the aerosol samples to the average topsoil composition in Australia (this study) and to the
105 averaged UCC composition (McLennan et al., 2001).

107 2. Material and methods

108 2.1 Aerosol collection and study site

109 kunanyi/Mount Wellington overlooks Hobart, the capital city of the Australian island state of
110 lutruwita/Tasmania. The mountain is in a strategic position for sampling one of the three major
111 atmospheric pathways in Australia (Baddock et al. 2015; Bowler 1976), where air-masses from
112 mainland Australia are transported south-eastwards over lutruwita/Tasmania (and our sampling
113 site, Figure 1) before reaching the Southern Ocean. This study uses aerosol filters collected on a
114 HiVOL 3000 air particulate sampler (Ecotech, Acoem, Melbourne, Australia) positioned at 1,271
115 m above sea level, on the summit of kunanyi/Mount Wellington. Filter samples have been
116 collected for Total Suspended Particulates (TSP) since September 2016, with each sample
117 representing a period ranging from a few days to 2 weeks, depending on weather conditions and
118 specific weather events, and allowing for sampler servicing and calibration. Samples suspected of
119 contamination or that were significantly wet at the time of recovery were discarded and sampling
120 was suspended in the wintertime of 2017, 2018 and 2019 for operational reasons. As a result, 125
121 aerosol samples were selected from the kunanyi/Mount Wellington atmospheric time-series
122 collection for this study (November 2016 - February 2022). The origin and concentration of aerosol
123 Fe in 80 samples from this dataset was previously reported in Perron et al. (2022), however the

124 present study differs in using total concentrations of Fe, Al, Th and Ti to calculate atmospheric
125 (dust) deposition fluxes and the associated seasonal and interannual trends at the sampling station.
126



127
128 **Figure 1.** Location of the aerosol sampling station at kunanyi/Mount Wellington in Tasmania (TAS). Black
129 dots display the locations of selected NGS soil samples in the Australian states of Western Australia
130 (WA), South Australia (SA) and Victoria (VIC) with identification numbers annotated (see Table S2).
131 Prevailing dust pathways of southeast Australia are displayed as green arrows adapted from Sprigg (1982)
132 and Mackie et al. (2008). The kati thanda/Lake Eyre (dashed line) and dhungala-barka/Murray-Darling
133 (solid line) geological basins are delineated in orange. Location of previous field studies that estimated dust
134 deposition fluxes are also indicated.

135

136 2.2 Aerosol leaching protocol

137 Laboratory work for aerosol and soil sample processing (sections 2.2 and 2.3) followed
138 GEOTRACES recommended procedures for ultra-trace sampling and analysis (Cutter et al., 2017).

139 All reagents were ultra-high purity (UHP) and either purchased (Baseline, SeaStar Chemicals) or
140 distilled in-house using instrument quality reagents (IQ grade, SeaStar Chemicals). Whatman W41
141 (203mm x 254mm paper sheets, Sigma-Aldrich) filters were acid washed in a series of 24h
142 hydrochloric acid (0.5 M HCl) baths and rinsed with UHP water to leach any impurities and reduce
143 the impact of the cellulose filter on the analysis of trace elements in aerosols (Perron et al., 2020a).
144 Perron et al. (2020a) suggested a 3-step leaching method to define trace metal concentrations and
145 solubility in aerosols taken from land-based stations in Australia (Strzelec et al., 2020a, 2020b)
146 and on research vessels operating around Australia and in the Southern Ocean (Perron et al., 2020b,
147 2021). Although samples were collected and analysed in batch over several years, the collection
148 and analysis of each batch of samples follow the same protocol and the resulting data was quality-
149 controlled against blanks, replicate analysis and Certified Reference Materials (Table S1).

150

151 One sub-sample of 47mm diameter was cut off each aerosol filter sheet collected at our sampling
152 station using a sharp titanium punch cutter (Perron et al., 2020). Sub-samples were successively
153 leached using UHP water (Milli-Q®, 18.2 MΩ) and 1.1 M ammonium acetate (10 mL, pH 4.7).
154 The remaining filter residue was then digested using a mixture of concentrated nitric acid (HNO₃,
155 1 mL) and concentrated hydrofluoric acid (HF, 0.25 mL) at 120°C for 12 hours (Perron et al.,
156 2020a). The sum of all three steps in the protocol provided the total concentration data for each
157 lithogenic tracer in aerosols which is used in this study (Perron et al., 2020a). Satisfactory
158 recoveries (>90%) were obtained for Al, Fe and Ti when applying the total metal digestion step of
159 the protocol to two reference materials, the Arizona Test Dust (ATD) (Morton et al., 2013) and
160 the GeoPT13 certified Koeln loess (International Association of Geoanalysts) (Potts et al., 2003)
161 (supplementary Table S1). A smaller recovery of 87% (using only certified reference material)
162 obtained for Th highlights the unique extraction and stability chemistry of the metal which our
163 protocol is not optimised for. Thorium concentrations are therefore likely to be slightly
164 underestimated in this study as discussed in section 3. Only total metal concentrations are
165 discussed in the present study.

166

167 2.3 Atmospheric deposition flux estimates

168 The total concentration of each lithogenic tracer in our samples was used to calculate single tracer-
169 dust deposition flux estimates. Additional measurements on the collected aerosols (e.g.; carbon

170 and major ion analysis) were not available for this study, so intrinsic calculation of the total aerosol
171 mass on each individual aerosol filter using these parameters was not possible.

172 In addition, due to the lack of necessary meteorological data to estimate particle deposition
173 velocities specific to our study site, a single coarse particle deposition velocity of 0.2 cm s^{-1} was
174 applied to trace metal-bearing dust deposition estimates based on the literature in similar study
175 regions (Baker et al., 2017; Perron et al., 2020b; Winton et al., 2015). In this study, “F(X)” denotes
176 the deposition flux estimate for the individual lithogenic tracer “X”. F(X) (in $\text{mg m}^{-2} \text{ d}^{-1}$) was
177 obtained following equation (1):

$$178 \quad F(X) = C_x * V_d \quad (1)$$

179 where X is the lithogenic tracer – Al, Fe, Th or Ti ; C_x is the total metal concentration (ng m^{-3}) in
180 aerosols and V_d is a constant deposition velocity of 1723 m d^{-1} (0.2 cm s^{-1}). It should be mentioned
181 that a factor of 3 uncertainty was previously attributed to the use of a set deposition velocity as it
182 does not account for specific particle size in different aerosol samples or for specific atmospheric
183 conditions such as humidity and wind speed at the collection time (Baker et al., 2016; Winton et
184 al., 2016; Duce et al, 1991).

185
186 Similar to other studies reported in the literature, a single-tracer dust (lithogenic) deposition flux
187 estimate, $F_{\text{Lith}(X)}$, was calculated by dividing F(X) by the average abundance ($[X]_{\text{UCC}}$, wt%) of the
188 element X in the UCC as reported in McLennan (2001); Al = 8.04%, Fe = 3.5%, Th = 1.07×10^{-3}
189 %, Ti = 0.41% following equation (2).

$$190 \quad F_{\text{Lith}(X)} = \frac{F(X) \times 100}{[X]_{\text{UCC}}} \quad (2)$$

191 While $F_{\text{Lith}(X)}$ estimates are solely based on the analysis of a single lithogenic tracer, a multi-tracer
192 dust deposition flux estimate, F_{LithAv} , was obtained by calculating the average of all four $F_{\text{Lith}(X)}$
193 (equation 3, N=4) for each individual aerosol sample.

$$194 \quad F_{\text{LithAv}} = \frac{\sum F_{\text{Lith}(X)}}{N} \quad (3)$$

195 Multi-tracer F_{LithAv} estimates were calculated using both the reported average UCC composition
196 (McLennan, 2001) and Australian soil measurements (see section 2.4 in this study) as references
197 for comparison.

198

199 2.4 Soil sampling and processing

200 Eleven topsoil (0-10 cm) samples were selected from the National Geochemical Survey of
201 Australia (NGSA) Project: Geochemical Atlas of Australia (Geoscience Australia), a continental-
202 scale geochemical survey covering most of Australia (Caritat and Cooper, 2011; Caritat, 2022).
203 In this study, soil samples originating from the southern part of Western Australia, from South
204 Australia and from Victoria were selected and analysed (Figure 1) as they likely better represent
205 particles entrained through the south-east Australian dust path towards our sampling station and
206 the Southern Ocean (Baddock et al., 2015, Supplementary Figure S1). These sources include the
207 geological basins of kati thanda/Lake Eyre and dhungala-barka/Murray-Darling, It should be
208 mentioned that no sample from New South Wales was used for this study although a large part of
209 the dhungala-barka/Murray-Darling basin is located in this state.

210
211 Ten milligrams of each soil sample was dry sieved through a 63 µm nylon screen to capture the
212 soil fraction fine enough to be entrained into the atmosphere (Strzelec et al., 2020a). The sieved
213 fraction was then processed through the same sequential leaching method described in section 2.2
214 (Perron et al., 2020a). Aerosol and soil leachates were analysed for a suite of elements, including
215 Al, Fe, Th and Ti, by Sector Field Inductively Coupled Plasma Mass Spectrometry (HR-ICP-MS,
216 Thermo Fisher Scientific, Element 2) at the Central Science Laboratory of the University of
217 Tasmania. Increased spectral resolution was employed to resolve major spectral interference
218 overlaps associated with analysis of Al, Fe and Ti. Further details on the ICP-MS analysis
219 procedure are provided in Perron et al. (2020a).

220

221 2.5 Atmospheric source tracking

222 The ratio between the total concentration of each lithogenic tracer of interest, T(X), and the total
223 Al concentration, T(Al), in individual aerosol samples was calculated and compared to the same
224 ratio in the average UCC reported in McLennan (2001) and in the average topsoil from
225 southeastern Australia (Section 2.3). The so-called enrichment factor (EF, equation 4) was used to
226 ascertain the lithogenic origin of Fe, Th and Ti in this study.

$$227 \quad EF = \frac{\frac{T(X)_{aerosol}}{T(Al)_{aerosol}}}{\frac{T(X)_{UCC}}{T(Al)_{UCC}}} \quad (4)$$

228 Using this approach, an EF value below 10 was considered to indicate a prevailing lithogenic
229 source origin for the metal tracers, while an EF exceeding the threshold value of 10 is associated

230 with an enrichment from non-lithogenic atmospheric sources such as anthropogenic combustion
 231 (Shelley et al., 2015; Perron et al., 2022). Reimann and Caritat (2005) warned about the biases
 232 associated with using a low EF threshold to identify anthropogenic sources due to the natural
 233 variability in the Earth’s crust composition, fractionation of elements during their emission to –
 234 and transport within – the atmosphere, and biogeochemical processes during and after aeolian
 235 transport. Here, a high EF threshold of 10 is adopted to account for such variability.
 236

237 **3. Results and discussion**

238 **3.1 Evaluating the lithogenic origin of the four tracers in aerosols**

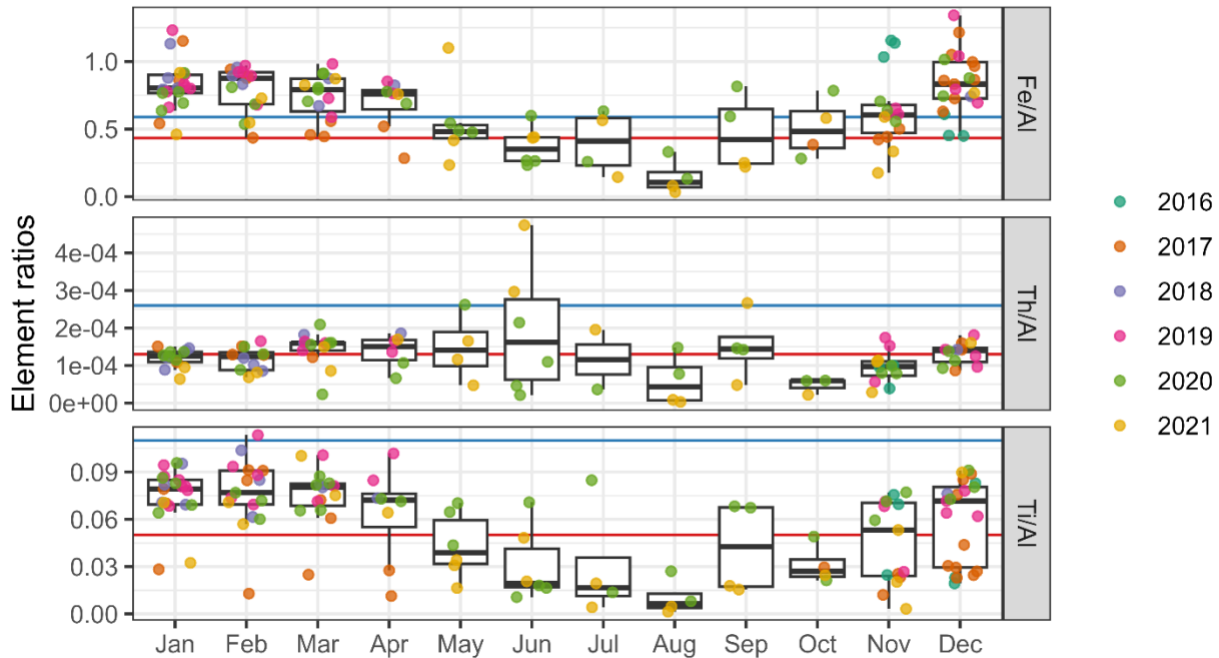
239 Enrichment Factors (EF) were calculated for Fe, Th and Ti measured in aerosols, and compared to
 240 the Australian soil samples selected from the NGSa (this study) and compared to averaged UCC
 241 composition from McLennan (2001) (Table 1). Calculated EF values were used to discard
 242 significant contributions of non-lithogenic sources to our lithogenic tracers in kunanyi/Mt
 243 Wellington aerosols as indicated by EF>10.
 244

Table 1. Comparison of mean Al, Fe, Th and Ti concentrations measured (ppm) in Australian soil samples (n = 11) compared to concentrations reported in the average UCC by McLennan (2001). Enrichment factors (EFs) calculated for Fe, Th and Ti (using Al as a reference) in aerosols collected at kunanyi/Mount Wellington (n = 125) are also displayed using both crustal references

| | UCC | Australian soils | | kunanyi/Mount Wellington aerosols | |
|-----------|-------|------------------|---------------|-----------------------------------|------------------|
| Al | 80400 | 38560 | | /UCC | /Australian soil |
| Fe | 35000 | 22616 | EF(Fe) | 1.6 ± 0.6 | 1.2 ± 0.5 |
| Th | 10.7 | 10.3 | EF(Th) | 1.3 ± 2.5 | 0.7 ± 1.2 |
| Ti | 4100 | 4313 | EF(Ti) | 1.2 ± 0.6 | 0.6 ± 0.6 |

245
 246 Overall, EFs close to 1 were measured for all aerosol samples, suggesting that the lithogenic tracers
 247 used in this study are indeed of a prevailing crustal origin. Using Australian soil concentration
 248 (Table 1 and supplementary Table S2) to calculate EFs resulted in values further away from the
 249 threshold of 10. In particular, EFs calculated using Australian soil data are closer to 1 for Fe and
 250 Th when compared to using average UCC values (McLennan, 2001). Indeed, underestimated Th
 251 measurements due to incomplete sample digestion (section 2.2) in our study result in a similar

252 underestimate of EF. Elemental ratio of Ti/Al in aerosol samples collected at kunanyi/Mt
 253 Wellington (Figure 2) were closer to the average ratio of the UCC, resulting in EF(Ti) closer to 1
 254 when compared to using average Australian soil measurement as a reference.
 255



256
 257 **Figure 2.** Boxplot of elemental ratios of Fe/Al (top), Th/Al (middle), and Ti/Al (bottom) in kunanyi/ Mt
 258 Wellington aerosol samples collected between 2016 – 2021, grouped according to month. Whiskers
 259 represent 1.5 times the interquartile range (75th – 25th percentile) beyond the boxes, while the upper, middle,
 260 and lower horizontal lines of the box represent the higher interquartile, median value and lower interquartile
 261 of the average monthly dataset, respectively. Colours represent each sample collection year. Horizontal red
 262 lines represent metal ratios in the average UCC (McLennan, 2001). Horizontal blue lines represent average
 263 metal ratios in the eleven selected NGSAs Australian soil samples (this study). Two Th outliers (May and
 264 June 2020) were excluded from the Th dataset and subsequent calculation for clarity.

265
 266 Mean Al and Fe concentrations measured in our Australian soil samples were both twice smaller
 267 than the average UCC values reported by McLennan (2001) while Ti and Th concentrations were
 268 similar within 10% (Figure 2 and supplementary Table S2). While Australian soil is known for its
 269 high Fe content (Mahowald et al., 2019, Strzelec et al., 2020a), a high soil heterogeneity across
 270 this vast country may explain such surprising observation. This resulted in calculated Th/Al and
 271 Ti/Al ratios higher for Australian soil samples while Fe/Al ratios remained similar compared to
 272 the average UCC.

273

274 Elemental ratios calculated for individual aerosol samples are summarised in the supplementary
275 Table S4. Both Fe/Al and Ti/Al ratios showed a clear seasonal trend, with higher ratios resembling
276 mean ratios measured in Australian soil samples (Fe/Al=0.59 and Ti/Al=0.11, Figure 2) in the
277 summertime (December-February) and lower Fe/Al and Ti/Al ratios closer to the average UCC
278 ratios (Fe/Al=0.435 and Ti/Al=0.05, McLennan, 2001) in wintertime (June-August, Figure 2).
279 Summertime Fe/Al ratios in kunanyi/Mt Wellington aerosols were slightly higher (Fe/Al =0.72)
280 than the Australian soil measurements. This can be explained by increased contribution of local
281 soil emission from Tasmania under drier weather conditions as the NGS database shows higher
282 Fe/Al ratio (on average 0.7, n=21 samples) in Tasmanian soil compared to other soil across
283 Australia (Caritat and Cooper, 2011; Caritat, 2022). While enhanced air-masses originating from
284 the Australian mainland cannot be observed in the summertime using HYSPLIT model
285 (supplementary Figure S1), the Australian Bureau of Meteorology reports increasing southwards
286 blowing winds at our sampling station from January through to March (supplementary Figure S2).
287 Such discrepancies emphasise the complex regional wind pattern influencing our sampling station
288 and highlight the need to consider other parameters such as seasonal changes in environmental
289 conditions at the source region when investigating aerosol entrainment and transport. Ti/Al ratios
290 were found to lie between our Australian soil (Ti/Al = 0.11) and UCC (Ti/Al = 0.05) references
291 from December through to May, then falling below the UCC ratio in the cooler months of the year.
292 This monthly variability indicates different lithogenic sources of Fe and Ti are likely to influence
293 the atmospheric loading at our sampling station throughout the year. The onset of the dust season
294 on the Australian mainland (October-November, Baddock et al., 2015) may explain part of the
295 summer (dusty) season atmospheric inputs at our kunanyi /Mt Wellington aerosol sampling station,
296 as evidenced by higher Fe/Al (and Ti/Al) ratios in aerosols. On the other hand, other atmospheric
297 sources (locally derived from Tasmania or from long-range transport over the Southern Ocean)
298 with a similar (lower) metal/Al signature than the UCC seem to prevail in our study region during
299 winter. However, the small number of aerosol samples available between May - October in our
300 study does not allow for accurate assessment of trends during the winter period. Much smaller
301 variability was observed for the Th/Al ratio calculated in kunanyi/Mt Wellington aerosols (mean
302 Th/Al = 0.00017) across the time-series, with an overall median ratio close to that of the UCC
303 (mean Th/Al = 0.00013) across most of the year except during August and October.

304

305 Differences between elemental ratios in soil and in aerosol samples may stem from atmospheric
 306 processes occurring during transport between source regions and the sampling site including the
 307 preferential settling of denser (e.g., oxyhydroxides) minerals over lighter minerals (e.g., clay), and
 308 from the mixing of different lithogenic air-masses during atmospheric transport. Analysis of a
 309 large set of soil samples, including more locations across Australia and particularly in Tasmania,
 310 as well as high resolution information on wind speed and direction at the sampling site and for the
 311 duration of the timeseries is necessary to better assess the relative contribution of different
 312 Australian dust sources to the lithogenic particulate loading at kunanyi/Mount Wellington.

313

314 3.2 Single tracer lithogenic particle fluxes at kunanyi/Mount Wellington: characteristics 315 and trends

316 Thorium and Ti are commonly used as tracers of lithogenic atmospheric deposition fluxes as they
 317 are almost exclusively derived from lithogenic material and have little reactivity or biological
 318 utility in the atmosphere (Boës et al., 2001; Ohnemus and Lam, 2015). While Al may be emitted
 319 to the atmosphere by anthropogenic sources, its prevailing source in the offshore atmosphere
 320 remains crustal material (Xu and Weber, 2021). Although Fe solubility vary following physico-
 321 chemical processes during the atmospheric transport, the soluble Fe fraction remains small
 322 compared to the total (mostly refractory) fraction of Fe delivered by dust. Hence, if all four tracers
 323 have a unique lithogenic source, the use of a multiple tracer lithogenic flux estimate can reduce
 324 the uncertainty associated with the variability of a single metal's concentration due to
 325 contamination, deviation from the UCC or secondary atmospheric inputs (Traill et al., 2022).

326

Table 2. Correlation coefficient (R^2) between tracer concentrations in kunanyi/Mount Wellington aerosols.

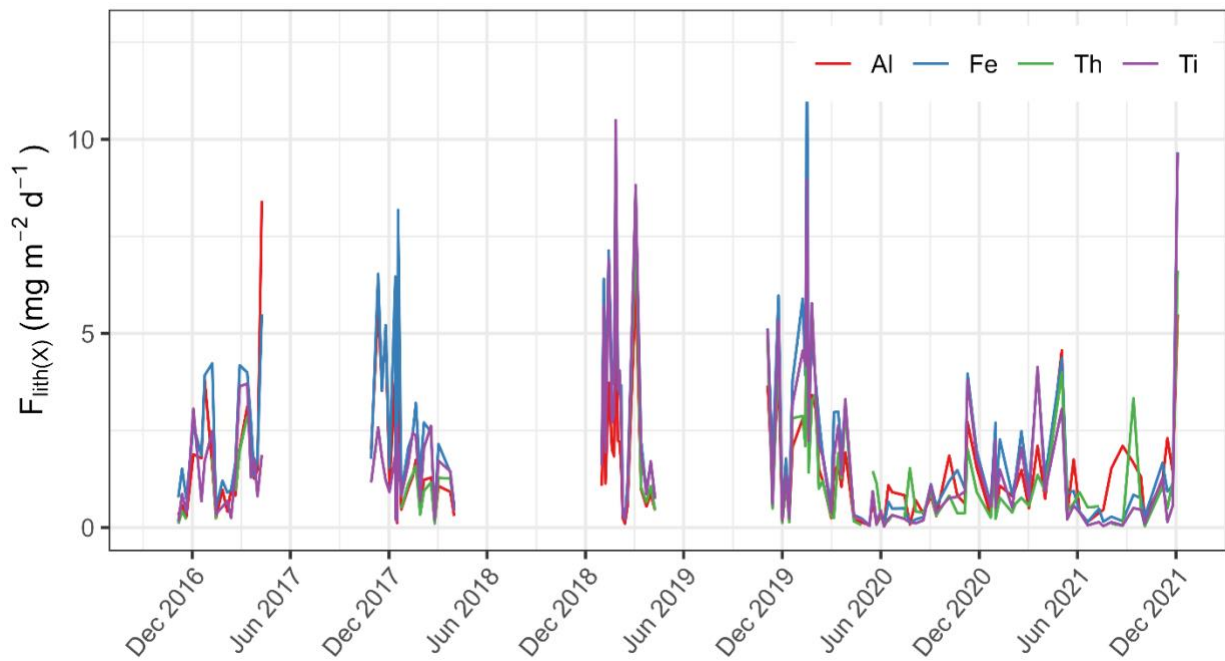
| | Al | Th | Fe | Ti |
|-----------|-----------|-----------|-----------|-----------|
| Al | 1 | - | - | - |
| Th | 0.90 | 1 | - | - |
| Fe | 0.87 | 0.82 | 1 | - |
| Ti | 0.74 | 0.84 | 0.83 | 1 |

327

328 A strong correlation (mostly $R^2 > 0.8$) was found between the total atmospheric concentrations of
 329 Al, Fe, Th and Ti in the individual samples (Table 2). The strongest correlation ($R^2 = 0.90$) was
 330 found between Al and Th and the weakest correlation ($R^2 = 0.74$) was found between total Ti and

331 Al concentrations in aerosols. Such strong correlations suggest that a common prevailing source
 332 may supply all four tracers to kunanyi/Mt Wellington sampling station. Australian soil samples
 333 collected in the state of Victoria and analyzed in this study also showed a good correlation between
 334 the four lithogenic tracers, with R^2 of 0.97, 0.74 and 0.73 for Fe, Th and Ti when compared to Al
 335 (based on Table S4 data). Such correlation was not found for soil samples from South Australia
 336 (only 2 soil samples from Western Australia). However, the small number of soil sample analysed
 337 in this study ($n=4$ for Victoria and $n=5$ in South Australia) is not sufficient to draw conclusion on
 338 the potential origin of metals in kunanyi/Mt Wellington aerosol samples. The NGS database
 339 available from Caritat and Cooper (2011) also shows a strong correlation (>0.70) between Fe and
 340 Al measurements in soil samples from New South Wales, South Australia and Tasmania using an
 341 aqua regia mineralization and x-ray florescence analysis protocol.

342



343

344 **Figure 3.** Individual tracer flux, $F_{Lith(X)}$ ($mg\ m^{-2}\ d^{-1}$), at the kunanyi/Mount Wellington aerosol sampling
 345 station from 2016 to 2021. Data points represent each aerosol mid-sampling period. Gaps in the time series
 346 are periods where samples were not collected due to logistical limitations (winters) or instrument
 347 maintenance. Here, $F_{Lith(X)}$ are calculated using the average UCC content for each metal as reported in
 348 McLennan (2001).

349

350 Dust deposition fluxes estimated using individual tracer (Al, Fe, Th, and Ti) concentrations
 351 measured in kunanyi/Mount Wellington aerosols, called $F_{lith(X)}$, showed similar variability
 352 throughout the time-series (2016-2021, Figure 3). Overall, the smallest $F_{lith(Th)}$ flux was estimated

353 using Th as a single lithogenic tracer, ranging between 0.03 and 7.8 mg m⁻² d⁻¹. The largest dust
354 flux was obtained using Fe as a lithogenic tracer and ranged between 0.05 and 12.7 mg m⁻² d⁻¹
355 (F_{lith(Fe)}, Figure 3). Lithogenic flux estimates calculated using Al and Ti concentrations in aerosols
356 ranged from 0.06 - 8.4 mg m⁻² d⁻¹ and from 0.03 - 10.5 mg m⁻² d⁻¹, for F_{lith(Al)} and F_{lith(Ti)},
357 respectively. Despite slight differences found between F_{lith(X)} estimates obtained using different
358 lithogenic tracers, the magnitude of the difference between the highest and lowest F_{lith(X)} estimates
359 varied by only a factor of 2, which reinforces the likelihood of a common prevailing atmospheric
360 source for all four tracers.

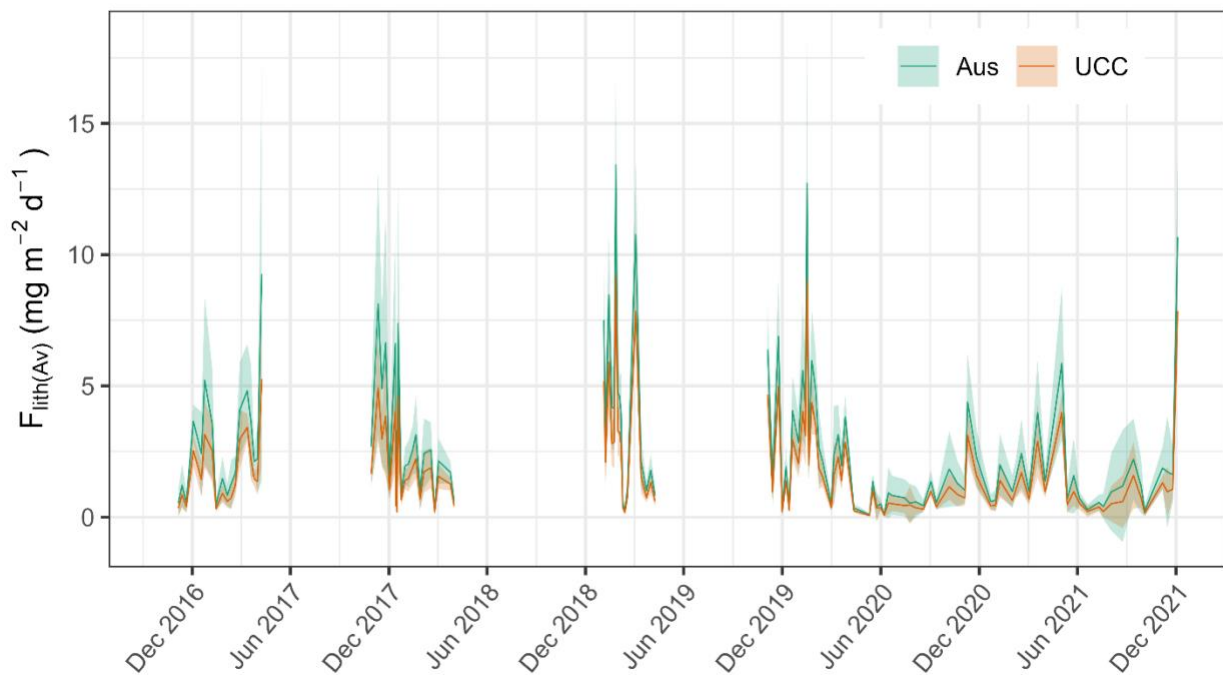
361
362 This finding corroborates work presented by Traill et al. (2022), where concentrations of all four
363 lithogenic tracers showed similar variabilities in marine sinking particles collected in the
364 subantarctic region of the Southern Ocean south of Tasmania (SOTS station). Similarly, Traill et
365 al. (2022) estimated higher lithogenic fluxes when using Fe as a lithogenic tracer and lower
366 lithogenic fluxes when using Th as a lithogenic tracer (Traill et al., 2022). Median F_{lith(X)} estimates
367 measured at the kunanyi/Mt Wellington sampling site (this study: 1.2, 1.7, 0.8 and 1.1 mg m⁻² d⁻¹
368 using Al, Fe, Th and Ti as individual lithogenic tracer, respectively) compares well with reported
369 dust deposition fluxes of 1.4 - 5 mg m⁻² d⁻¹ estimated by models in the study region (Jickells et al.,
370 2005; Mahowald et al., 2005; Weis et al., 2024) and other Southern Hemisphere dust fluxes <2.7
371 mg m⁻² d⁻¹ reported off the coasts of South Africa and South America, away from major dust
372 sources (Menzel Barraqueta et al., 2019). Our flux estimates are smaller than mineral dust
373 deposition estimates of 4.0 - 25.0 mg m⁻² d⁻¹ (based on Ti concentration in aerosols) reported by
374 Strzelec et al. (2020a) in Western Australia, much closer to large Australian deserts.

375
376 Overall, maximum F_{Lith(X)} estimates in our study were calculated during austral summer months
377 (roughly December – March). Different metals are observed to dominate the summer F_{Lith(X)} peak
378 each year, with Al showing the highest F_{Lith(X)} flux in summer 2016/17 (8.4 mg m⁻² d⁻¹), Fe in
379 2017/18 (8.2 mg m⁻² d⁻¹) and in 2019/20 (12.7 mg m⁻² d⁻¹), and Ti in 2018/19 (10.5 mg m⁻² d⁻¹)
380 and in 2021/22 (9.6 mg m⁻² d⁻¹). This may be due to variabilities in the nature and composition of
381 the dominant dust source arriving at the sampling site each year, including the impact of dust-
382 containing fire emissions during the summer seasons 2018/19 and 2019/20 (Perron et al. 2022).

383

384 3.3 Multi tracer particle flux

385 All four tracers (Al, Fe, Th, and Ti) measured in kunanyi/Mount Wellington aerosols showed a
386 strong correlation with one another and a similar variability over time (section 3.1), suggesting
387 that they originated from a single terrestrial source. This supports the approach taken in this study
388 whereby a multi-tracer lithogenic deposition flux, called F_{LithAv} , is estimated by averaging $F_{Lith(x)}$
389 fluxes obtained using each of the four tracers for each sample. The resulting F_{LithAv} estimated at
390 our station between 2016 and 2021 is displayed in Figure 4 and provides a more robust estimate
391 of deposition flux by smoothing variability between tracers (displayed in Figure 3). Individual and
392 average lithogenic flux estimates ($F_{Lith(x)}$ and F_{LithAv} , respectively) calculated in this study are
393 summarised for individual samples in the supplementary Tables S5 and S6, respectively.



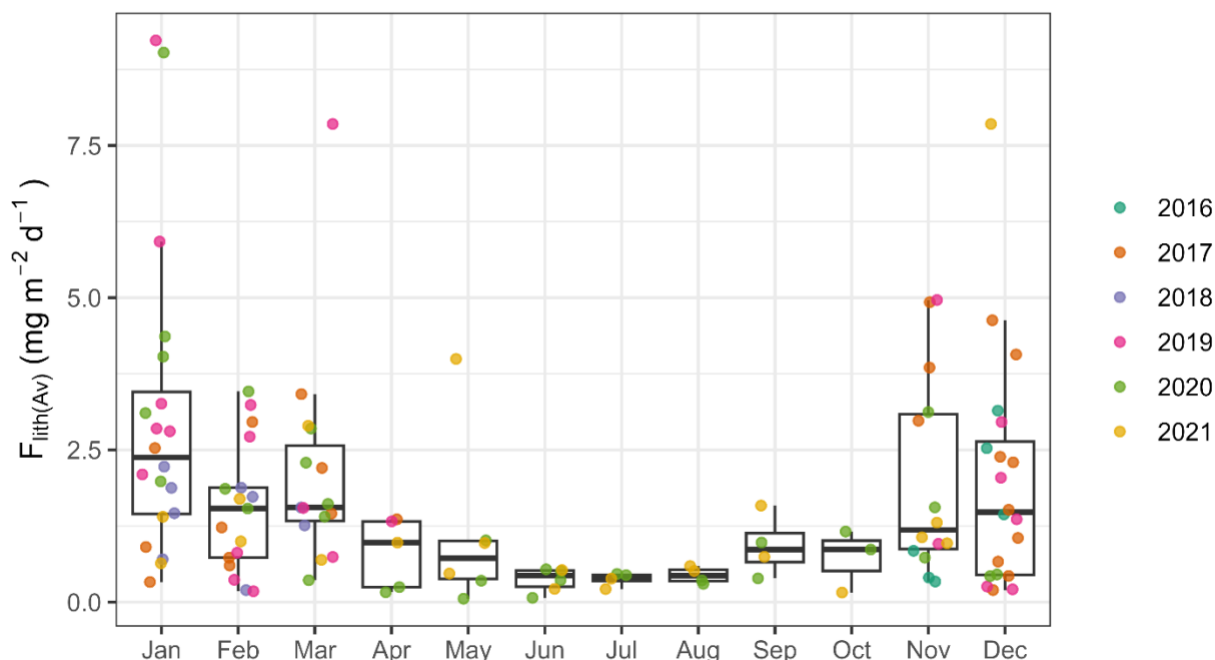
394
395 **Figure 4.** Multi-tracer lithogenic flux estimate, F_{LithAv} , expressed in $\text{mg m}^{-2} \text{d}^{-1}$, corresponding to the average
396 of all individual tracer fluxes ($F_{Lith(x)}$) calculated based on the lithogenic composition of the UCC (orange
397 colour) and that of the eleven Australian soil samples measured in this study (green colour). Shadings
398 represent \pm one F_{LithAv} standard deviation of the average (solid lines).
399

400 A mean F_{LithAv} value of $1.8 \pm 1.3 \text{ mg m}^{-2} \text{d}^{-1}$ was calculated based on the analysis of aerosol samples
401 collected between 2016 and 2021 at kunanyi/Mt Wellington (Tasmania, Figure 4 orange colour).
402 Throughout our time series, the highest F_{LithAv} values were observed in January 2019 and 2020,
403 with flux peaks reaching 9.2 in January 2019 and 9.0 $\text{mg m}^{-2} \text{d}^{-1}$ in January 2020, respectively.
404 Noticeable peak fluxes of 7.9 $\text{mg m}^{-2} \text{d}^{-1}$ also occurred in early March 2019 and in mid-December

405 2021. Extended periods of low F_{LithAv} estimates ($\leq 0.5 \text{ mg m}^{-2} \text{ d}^{-1}$) were observed during the two
406 austral winter periods sampled, with a minimum flux of $0.06 \text{ mg m}^{-2} \text{ d}^{-1}$ reached in May 2020
407 (Figure 4). There is therefore an apparent seasonal trend in dust deposited at the kunanyi/Mt
408 Wellington site, with higher F_{LithAv} observed in warmer periods (November - March) and lower
409 fluxes in cooler periods of the year (May - August). It should be mentioned that a mean F_{LithAv}
410 value of $2.7 \pm 1.9 \text{ mg m}^{-2} \text{ d}^{-1}$ is estimated when using the average metal content in Australian soil
411 analyzed in this study (Figure 4 green colour). Indeed, while Th and Ti contained in our eleven
412 Australian soil samples show similar concentrations (within 10%) as in the average UCC
413 (McLennan, 2001), Al and Fe concentrations in these local soil samples differ by 52 and 35%,
414 respectively. This result in higher F_{LithAv} estimated using Australian soil data (Figure 4).

415 The mean F_{LithAv} observed in this study, of $1.8 \text{ mg m}^{-2} \text{ d}^{-1}$ when using the average UCC and 2.7
416 $\text{mg m}^{-2} \text{ d}^{-1}$ when using the average Australian soil measurement (Table S5), fall within the dust
417 deposition range of $1.1 - 5.5 \text{ mg m}^{-2} \text{ d}^{-1}$ reported by models in southeastern Australia, which
418 account for soil erodibility, soil particle size distribution and wind friction velocity (Albani et al.,
419 2014; Weis et al., 2024). In the Southern Ocean south of Tasmania, smaller mineral dust fluxes of
420 $0.37 \text{ mg m}^{-2} \text{ d}^{-1}$ and $1.0 \text{ mg m}^{-2} \text{ d}^{-1}$ were reported based on aerosol Fe measurements at sea, particle
421 size and surface wind speed (Bowie et al., 2009) and based on Al, Fe, Th and Ti measurements in
422 marine sinking particles (Traill et al., 2022), respectively. Traill et al. (2022) reported a similar
423 annual variability in lithogenic deposition flux at SOTS between 2011 and 2018, with minimum
424 F_{LithAv} around $0.5 \text{ mg m}^{-2} \text{ d}^{-1}$ in July-September and an earlier dust deposition peak (compared to
425 our study) in November-December, up to $2.5 \text{ mg m}^{-2} \text{ d}^{-1}$. Strzelec et al. (2020a) also reported (up
426 to 6 times) higher mineral dust fluxes in warmer months compared to cooler months based on Ti
427 analysis in aerosols from Western Australia. In particular, the two summer seasons showing F_{LithAv}
428 over $9.0 \text{ mg m}^{-2} \text{ d}^{-1}$ correspond to large bushfire seasons in Tasmania and in Australian mainland
429 upwind from Tasmania, respectively (Perron et al., 2022). Indeed, fire events are known to
430 exacerbate dust entrainment into the atmosphere both during (pyro convective updrafts) and post
431 (burnt ground) fire event (Hamilton et al., 2022). It is worth noting that F_{LithAv} estimated using
432 Australian soil measurements (this study) fall closer to the mean reported estimate found in the
433 literature while using the average UCC value result in lower-end F_{LithAv} estimate compared to the
434 literature. While F_{LithAv} estimated using the average UCC may present an advantage in being more

435 comparable with other studies worldwide, F_{LithAv} estimated using Australian soil data may be more
 436 relevant for validating model outputs as it likely better represents true deposition fluxes in our
 437 study region. Overall, the choice of one or the other crustal source result in up to a factor 2
 438 difference in the calculated F_{LithAv} .



439
 440 **Figure 5.** Monthly F_{LithAv} estimates, in $mg\ m^{-2}\ d^{-1}$, based on lithogenic tracer analysis in aerosol samples
 441 collected between 2016-2021 at the kunanyi/Mt Wellington site. Individual (weekly) samples are shown
 442 as dots and the colour code represents each collection year. Whiskers represent 1.5 times the interquartile
 443 range (75th – 25th percentile) beyond the boxes, while the upper, middle, and lower horizontal lines of the
 444 box represent the higher interquartile, median value and lower interquartile of the average monthly
 445 dataset, respectively.

446 Greatest F_{LithAv} fluxes are annually observed during the austral summer (December - March),
 447 with median F_{LithAv} of $2.4\ mg\ m^{-2}\ d^{-1}$ in January and around $1.4\ mg\ m^{-2}\ d^{-1}$ in December,
 448 February and March across all years (Figure 5). This tendency aligns with higher frequency of
 449 dust storms occurring in Australia’s main geological basins during warmer months (late austral
 450 spring and summer), resulting in higher dust deposition fluxes (O’Loingsigh et al., 2017). The
 451 summers of 2017/2018 (Nov-Dec), 2018/19 (Jan-Feb) and 2019/20 (Dec-Feb) had especially
 452 high F_{LithAv} fluxes compared to other summer periods in the time-series (Figure 5). These
 453 observations are consistent with the year 2017 being identified as the third driest year since
 454 records have been kept in Australia (Steffen et al., 2018), and the two following summer periods

455 being identified as strong bushfire years, across Tasmania in 2018/2019, and across southeast
456 Australia in 2019/2020 (Perron et al., 2022). Relatively smaller peaks were observed during the
457 summer of 2020/21 and, to a lesser extent, during the 2016/17 summer (Figure 5). This may
458 reflect two wetter summer periods under the influence of El Niño Southern Oscillation positive
459 phase (La Niña), where increased moisture in the topsoil restricted particles from being eroded
460 and entrained by air masses (Bureau of Meteorology, 2022). In addition, fewer bushfire
461 emissions during these two wetter summer periods may have resulted in less dust emissions due
462 to increased vegetation cover on the soil (Bureau of Meteorology, 2022). Wetter summer seasons
463 may also explain a shift in F_{lithAv} peaks towards the end of the summer seasons 2016/17 and
464 2020/21 (February - March) compared to the December-January $F_{\text{lith(Av)}}$ peak observed in
465 2017/18, 2018/19, and 2019/20 (Figure 5).

466

467 4. Conclusions

468 This study explores the seasonal and interannual variability of the lithogenic deposition flux using
469 analysis of Al, Fe, Th, and Ti (as lithogenic tracers) in aerosol samples collected at kunanyi/Mt
470 Wellington (Tasmania, Australia). Enrichment factors close to 1 and elemental ratios similar to
471 those measured in soil samples collected in Australian dust source regions confirmed the crustal
472 origin of all four tracers. Deposition fluxes, $F_{\text{Lith(X)}}$, calculated using each tracer individually
473 showed small differences, of a factor 2 on average, between one another throughout the 2016-2021
474 time series. This study suggests the use of a multi-tracer (averaged) dust deposition flux estimate
475 as a more robust method to account for variability of individual tracers in aerosols.

476 The mean F_{lithAv} of $1.8 \text{ mg m}^{-2} \text{ d}^{-1}$ calculated in this study across the 2016-2021 time-series is
477 consistent with earlier lithogenic deposition fluxes reported in the literature. Dust flux maxima (up
478 to $9.2 \text{ mg m}^{-2} \text{ d}^{-1}$) were consistently observed during the austral summer, while minimum annual
479 F_{lithAv} (down to $0.06 \text{ mg m}^{-2} \text{ d}^{-1}$) were estimated in the winter. Overall, individual year F_{lithAv} fluxes
480 aligned well with the occurrence of known dust and bushfire events in the summertime as well as
481 other global meteorological events such as El Niño Southern Oscillation (ENSO) which drive the
482 weather patterns across southeast Australia.

483 Dust deposition fluxes calculated in this study hold some uncertainties of a factor 3 and a factor 2
484 due to the use of a set deposition velocity and the assumption of metal abundance as per the average
485 UCC, respectively. While using the averaged UCC to calculate F_{LithAv} may present an advantage
486 in being more comparable with other studies worldwide, we show that F_{LithAv} estimates (0.09 –
487 13.4 mg m⁻² d⁻¹) calculated using metal abundance in Australian soils are in better agreement with
488 dust fluxes reported by global models in our study region. Therefore, understanding local soil
489 composition is essential to estimating dust deposition fluxes in different study regions. Overall,
490 the uncertainty in field-based dust deposition flux estimates likely remain smaller than
491 uncertainties associated with model parametrization.

492 As dust deposition is now being recognized as a major source of vital micro-nutrients such as Fe
493 to the Southern Ocean, accurately quantifying dust fluxes is vital to understanding primary
494 production in the Southern Ocean and how this may change under future climate scenarios. Our
495 observed dust flux maxima in austral summer may also provide a much-needed regional pulse of
496 nutrients to phytoplankton when water column nutrients are being depleted through the growing
497 season.

498 Additional observations covering a wider geographical area and greater temporal coverage
499 (including time-series stations and winter sampling periods) are required to better constrain
500 seasonal and interannual variability. Our study adds vital data to the relatively few field-based dust
501 deposition flux estimates available to validate model outputs, especially for Southern hemisphere
502 dust sources (including Australia) which greatly vary in nature and composition.

503

504 Author contributions

505 A.R.B. was responsible for project conceptualisation, funding acquisition, resources and
506 supervision. M.M.G.P. was responsible for part of the sample collection, sample processing, data
507 interpretation, processing and curation as well as for manuscript drafting. S.M was responsible for
508 part of the sample collection and analysis, and for laboratory supervision. T.H was responsible for
509 data curation. C.N was responsible for the analysis of soil samples. C.H was responsible for part
510 of the sample collection, sample processing, data curation and the original draft writing. A.T. was
511 responsible for instrumental analysis. P.dC. was responsible for part of the sample collection and
512 data curation. M.S. was responsible for part of the sample collection and sample processing. All

513 authors were responsible for data interpretation and validation and reviewing and editing the
514 manuscript.
515

516 **Competing interest**
517 There are no conflicts to declare.
518

519 **Code/ Data availability**
520 All data produced in this study is available either in the manuscript or in the supplementary files.
521

522 **Acknowledgements**

523 A.R.B would like to thank the Australian Research Council (ARC) for part funding this work under
524 grants FT130100037 and DP190103504. The Australian Antarctic Program Partnership (AAPP)
525 is also acknowledged for support of laboratory costs as part of the Antarctic Science Collaboration
526 Initiative (ASCI000002). Access to ICP-MS instrumentation was made possible through ARC
527 LIEF funding (LE0989539). M.M.G.P was partly supported by ISblue project, Interdisciplinary
528 graduate school for the blue planet (ANR-17-EURE-0015) and co-funded by a grant from the
529 French government under the program "Investissements d'Avenir" embedded in France 2030. Soil
530 samples were provided by The South Australia Drill Core Reference Library and the Geological
531 Survey of South Australia, within the Department for Energy and Mining; many thanks to Anna
532 Petts for assisting with legacy soil data selection and retrieval. The National Geochemical Survey
533 of Australia, which provided the topsoil samples from Western Australia, South Australia, and
534 Victoria, was a collaboration between Federal, States, and Northern Territory geological surveys
535 led by Geoscience Australia (GA) and funded by the Australian Government's Onshore Energy
536 Security Program (2006-2011). We thank GA for making those samples available for the present
537 study. We are deeply grateful to Dr Marc Mallet (University of Tasmania) for providing advice on
538 air-mass trajectory analysis.
539

540 **Acknowledgment to country**

541 Before the white settlement of lutruwita/Tasmania, kunanyi/Mount Wellington was a prominent
542 feature in the lives of the Moomairremener people for thousands of years and continues to be. We
543 pay our respects to elders' past, present and emerging and are thankful to have been able to study
544 this region.

545

546 References

- 547 Albani S, et al. 2014, 'Improved dust representation in the Community Atmosphere Model', *Journal of*
548 *Advances in Modeling Earth Systems*, vol. 6, no. 3, pp. 541–570, doi/10.1002/2013MS000279.
- 549 Anderson RF, et al. 2016, 'How well can we quantify dust deposition to the ocean?', *Philosophical*
550 *Transactions of the Royal Society A: Mathematical, Physical and Engineering Sciences*, vol. 374, no.
551 2081, p. 20150285, doi/10.1098/rsta.2015.0285.
- 552 Baddock M, et al. 2015, 'Drivers of Australian dust: a case study of frontal winds and dust dynamics in
553 the lower lake Eyre basin', *Earth Surface Processes and Landforms*, vol. 40, no. 14, pp. 1982–1988,
554 doi.org/10.1002/esp.3773
- 555 Baker AR, et al. 2016, 'Trace element and isotope deposition across the air–sea interface: progress and
556 research needs', *Philosophical Transactions of the Royal Society A: Mathematical, Physical and*
557 *Engineering Sciences*, vol. 374, no. 2081, p. 20160190, doi/10.1098/rsta.2016.0190.
- 558 Baker AR, et al. 2017, 'Observation- and model-based estimates of particulate dry nitrogen deposition to
559 the oceans', *Atmospheric Chemistry and Physics*, vol. 17, no. 13, pp. 8189–8210, doi.org/10.5194/acp-17-
560 8189-2017.
- 561 Baker AR, Li M and Chance R, 2020, 'Trace Metal Fractional Solubility in Size-Segregated Aerosols
562 From the Tropical Eastern Atlantic Ocean', *Global Biogeochemical Cycles*, vol. 34, no. 6, p.
563 e2019GB006510, doi/10.1029/2019GB006510.
- 564 Bindu G, et al. 2016, 'Pattern of aerosol mass loading and chemical composition over the atmospheric
565 environment of an urban coastal station', *Journal of atmospheric and solar-terrestrial physics*,
566 vol. 138, 10.1016/j.jastp.2016.01.004
- 567 Bowie AR, et al. 2009, 'Biogeochemical iron budgets of the Southern Ocean south of Australia:
568 Decoupling of iron and nutrient cycles in the subantarctic zone by the summertime supply', *Global*
569 *Biogeochemical Cycles*, vol. 23, no. 4, doi/10.1029/2009GB003500.
- 570 Bowler JM, 1976, 'Aridity in Australia: Age, origins and expression in aeolian landforms and sediments',
571 *Earth-Science Reviews*, vol. 12, no. 2–3, pp. 279–310, doi.org/10.1016/0012-8252(76)90008-8.
- 572 Bureau of Meteorology 2022, *ENSO Outlook*, www.bom.gov.au/climate/enso/outlook.
- 573 Caritat P de and Cooper M, 2011, *National Geochemical Survey of Australia: The Geochemical Atlas of*
574 *Australia*, dx.doi.org/10.11636/Record.2011.020.
- 575 de Caritat P de, 2022, 'The National Geochemical Survey of Australia: review and impact',
576 *Geochemistry: Exploration, Environment, Analysis*, vol. 22, geochem2022-032,
577 doi.org/10.1144/geochem2022-032.
- 578 Crawford J, et al. 2021, 'Fingerprinting Australian soils based on their source location', *Atmospheric*
579 *Pollution Research*, vol. 12, no. 3, pp. 173–183, doi.org/10.1016/j.apr.2021.01.007.

580 Cudahy T, et al. 2016, ‘Satellite-derived mineral mapping and monitoring of weathering, deposition and
581 erosion’, *Scientific Reports*, vol. 6, p. 23702, doi.org/10.1038/srep23702.

582 Cutter G, et al. 2017, ‘Sampling and Sample-handling Protocols for GEOTRACES Cruises’, Version 3.0.

583 De Deckker P, 2019, ‘An evaluation of Australia as a major source of dust’, *Earth-Science Reviews*, vol.
584 194, pp. 536–567, doi.org/10.1016/j.earscirev.2019.01.008.

585 Duce RA, et al. 1991, ‘The atmospheric input of trace species to the world ocean’, *Global*
586 *Biogeochemical Cycles*, vol. 5, no. 3, pp. 193–259, doi/10.1029/91GB01778.

587 Hamilton DS, et al. 2022, ‘Earth, Wind, Fire, and Pollution: Aerosol Nutrient Sources and Impacts on
588 Ocean Biogeochemistry’, *Annual Review of Marine Science*, vol. 14, no. 1, pp. 303–330,
589 doi/10.1146/annurev-marine-031921-013612.

590 Ito A, et al. 2020, ‘Evaluation of aerosol iron solubility over Australian coastal regions based on inverse
591 modeling: implications of bushfires on bioaccessible iron concentrations in the Southern Hemisphere’,
592 *Progress in Earth and Planetary Science*, vol. 7, no. 1, p. 42, doi.org/10.1186/s40645-020-00357-9.

593 Jickells T, et al. 2005, ‘Global Iron Connections Between Desert Dust, Ocean Biogeochemistry, and
594 Climate’, *Science*, vol 308, p. 67-71, doi/10.1126/science.1105959.

595 Mackie DS, et al. 2008, ‘Biogeochemistry of iron in Australian dust: From eolian uplift to marine
596 uptake’, *Geochemistry, Geophysics, Geosystems*, vol. 9, no. 3, doi/10.1029/2007GC001813.

597 Mahowald NM, et al. 2005, ‘Atmospheric global dust cycle and iron inputs to the ocean’, *Global*
598 *Biogeochemical Cycles*, **19**(4), GB4025. doi.org/10.1029/2004GB002402.

599 Mahowald NM, et al. 2006, ‘Change in atmospheric mineral aerosols in response to climate: Last glacial
600 period, preindustrial, modern, and doubled carbon dioxide climates’, *Journal of Geophysical Research:*
601 *Atmospheres*, vol. 111, no. D10, doi/10.1029/2005JD006653.

602 Mahowald NM, et al. 2009, ‘Atmospheric Iron Deposition: Global Distribution, Variability, and Human
603 Perturbations’, *Annual Review of Marine Science*, vol. 1, no. 1, pp. 245–278,
604 doi/10.1146/annurev.marine.010908.163727.

605 McLennan SM, 2001, ‘Relationships between the trace element composition of sedimentary rocks and
606 upper continental crust’, *Geochemistry, Geophysics, Geosystems*, vol. 2, no. 4,
607 doi/10.1029/2000GC000109.

608 Menzel Barraqueta J-L, et al. 2019, ‘Atmospheric deposition fluxes over the Atlantic Ocean: a
609 GEOTRACES case study’, *Biogeosciences*, 16, doi.org/10.5194/bg-16-1525-2019.

610 Ohnemus DC and Lam PJ, 2015, ‘Cycling of lithogenic marine particles in the US GEOTRACES North
611 Atlantic transect’, *Deep Sea Research Part II: Topical Studies in Oceanography*, vol. 116, pp. 283–302,
612 doi.org/10.1016/j.dsr2.2014.11.019.

613 O’Loingsigh T, et al. 2017, ‘Sources and pathways of dust during the Australian “Millennium Drought”
614 decade’, *Journal of Geophysical Research: Atmospheres*, vol. 122, no. 2, pp. 1246–1260,
615 doi/10.1002/2016JD025737.

616 Perron MMG, et al. 2020a, ‘Assessment of leaching protocols to determine the solubility of trace metals
617 in aerosols’, *Talanta*, vol. 208, p. 120377, doi.org/10.1016/j.talanta.2019.120377.

618 Perron MMG, et al. 2020b, ‘Origin, transport, and deposition of aerosol iron to Australian coastal waters’,
619 *Atmospheric Environment*, vol. 228, p. 117432, doi.org/10.1016/j.atmosenv.2020.117432.

620 Perron MMG, et al. 2021, ‘Atmospheric inputs of volcanic iron around Heard and McDonald Islands, Southern
621 ocean’, *Environmental Science : Atmospheres*, vol 1, p 508-517, doi.org/10.1039/D1EA00054C.

622 Perron MMG, et al. 2022, ‘Trace elements and nutrients in wildfire plumes to the southeast of Australia’,
623 *Atmospheric Research*, vol. 270, p. 106084, doi.org/10.1016/j.atmosres.2022.106084.

624 Reimann C, and P Caritat de. 2005. ‘Distinguishing between natural and anthropogenic sources for
625 elements in the environment: regional geochemical surveys versus enrichment factors’, *Science of the
626 Total Environment*, vol 337, p 91-107, doi.org/10.1016/j.scitotenv.2004.06.011

627 Shelley RU, Morton PL and Landing WM 2015, ‘Elemental ratios and enrichment factors in aerosols
628 from the US-GEOTRACES North Atlantic transects’, *Deep Sea Research Part II: Topical Studies in
629 Oceanography*, vol. 116, pp. 262–272, doi.org/10.1016/j.dsr2.2014.12.005.

630 Sprigg RC. 1982, ‘Some stratigraphic consequences of fluctuating Quaternary sea levels and related wind
631 regimes in southern and central Australia, In: *Quaternary dust mantles, China, New Zealand and
632 Australia*. Wasson RJ. ed. pp. 211-240. Australian National University: Canberra.

633 Steffen W, Rice M and Alexander D 2017, ‘Another record-breaking year for heat and extreme weather’,
634 Climate Council of Australia, ISBN 978-1-925573-47-3.

635 Strzelec M, et al. 2020a, ‘Atmospheric Trace Metal Deposition from Natural and Anthropogenic Sources
636 in Western Australia’, *Atmosphere*, vol. 11, no. 5, p. 474, doi.org/10.3390/atmos11050474.

637 Strzelec M, et al. 2020b, ‘Atmospheric Trace Metal Deposition near the Great Barrier Reef, Australia’,
638 *Atmosphere*, 11(4), 394, doi.org/10.3390/atmos11040390.

639 Strzelec M, 2020c, ‘Source characterisation of atmospheric trace metal deposition around Australia’.
640 University of Tasmania. Thesis. Doi.org/10.25959/100.00035895.

641 Traill CD, et al. 2022, ‘Lithogenic Particle Flux to the Subantarctic Southern Ocean: A Multi-Tracer
642 Estimate Using Sediment Trap Samples’, *Global Biogeochemical Cycles*, vol. 36, no. 9,
643 doi/10.1029/2022GB007391.

644 Vecchio M.A., et al. 2024, ‘Provenance of mineral dust deposited on Antarctica over the last sixty years
645 by strontium isotopic analysis of snow from Dome C’, *Atm. Env.*, vol 338,
646 doi:10.1016/j.atmosenv.2024.120850

647 Weis J, et al. 2022, ‘Southern Ocean phytoplankton stimulated by wildfire emissions and sustained by
648 iron recycling’, *Geophys. Res. Lett.*, vol. 49, p. 1–11, doi:10.1029/2021gl097538

649 Weis J., et al. 2024, ‘One-third of Southern Ocean productivity is supported by dust deposition’, *Nature*,
650 vol 629, pp. 603–608, doi:10.1038/s41586-024-07366-4

651 Winton VHL, et al. 2015, ‘Fractional iron solubility of atmospheric iron inputs to the Southern Ocean’,
652 *Marine Chemistry*, vol. 177, pp. 20–32, doi.org/10.1016/j.marchem.2015.06.006.

653 Winton VHL, et al. 2016, ‘Dry season aerosol iron solubility in tropical northern Australia’, *Atmospheric
654 Chemistry and Physics*, vol. 16, no. 19, pp. 12829–12848, doi.org/10.5194/acp-16-12829-2016.

655 Xu H., and Weber T. 2021, ‘Ocean dust deposition rates constrained in a data-assimilation model of the
656 marine aluminum cycle’, *Global Biogeochemical Cycles*, vol 35 no. 9. doi.org/10.1029/2021GB007049